

Supporting Information for

Ultrasonic Preparation of Porous Silica-Dye Microspheres: Sensors for Quantification of Urinary Trimethylamine *N*-oxide

Zheng Li and Kenneth S. Suslick*

Department of Chemistry, University of Illinois at Urbana–Champaign, 600 S. Mathews Avenue, Urbana,
Illinois 61801, United States
E-mail: ksuslick@illinois.edu

Table of Contents

1. Reagents and Experimental	Table S1 & S2	p. S2
2. Methodology and Material Characterization	Figure S1–S7	p. S3
3. Data Validation and Analysis	Figure S8–S10	p. S6

Table S1. Chemically responsive dyes incorporated into each of 13 different organically modified silica microspheres.

Spot #	Name
1	Ethanone
2	α -Naphthyl Red
3	Tetraiodophenolsulfonephthalein
4	Fluorescein
5	Bromocresol Green
6	Bromocresol Purple
7	Bromophenol Red
8	Rosolic Acid
9	Bromopyrogallol Red
10	Pyrocatechol Violet
11	LiNO ₃ + Cresol Red
12	AgNO ₃ + Bromophenol Blue
13	AgNO ₃ + Bromocresol Green

Table S2. Formulations of a simulated urine sample, including volatile amines, non-volatile organic, and inorganic components.

	Components	Concentration (mM)
Amino additives	TMA	0.002 ^a
	NH ₃	8 ^b
	MA	0.03 ^c
	DMA	0.3 ^{c,d}
	EA	0.02 ^c
	MEA	<0.0004 ^c
Organic compounds	TMAO	0.3 ^b
	creatinine	10 ^e
	urea	170 ^{f,h}
	uric acid	0.4 ^h
Inorganic salts	NaCl	116 ^g
	NH ₄ Cl	43 ^g
	Na ₂ HPO ₄	9 ^g
	KH ₂ PO ₄	18 ^g
	Na ₂ SO ₄	17 ^g

a) Wolrath, H. *et. al.* *APMIS* **2005**, *113*, 513-516; b) Tang, W. N. *et. al.* *Engl. J. Med.* **2013**, *368*, 1575-1584; c) Lundh, T. *et. al.* *J. Chromatogr.* **1993**, *617*, 191-196; d) Tsikas, D. *et. al.* *J. Chromatogr. B* **2007**, *851*, 229-239; e) Barr, D. B. *et. al.* *Environ. Health. Perspect.* **2005**, *113*, 192-200; f) Pandey, S. *et. al.* *ACS Sens.* **2016**, *1*, 55-62; g) <http://www.pickeringtestsolutions.com/catalog/AU.php>; h) Kim, W. *et. al.* *PLoS ONE* **2013**, *8*, e62437.

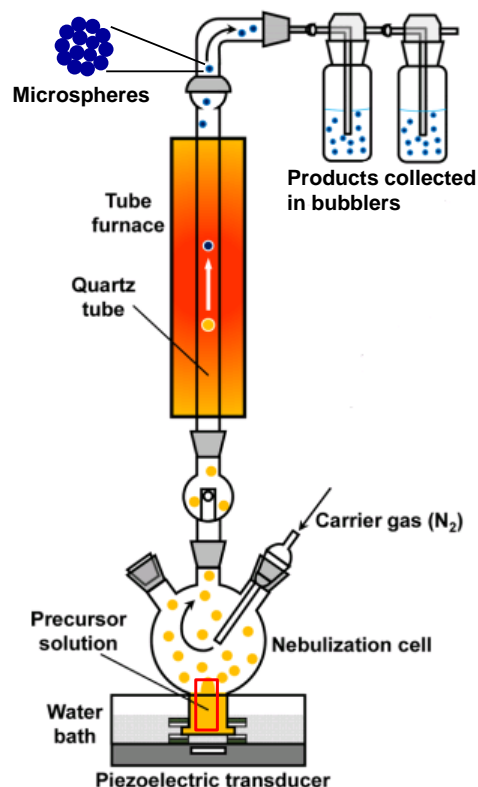


Figure S1. Ultrasonic spray synthesis of organically modified silica silica-dye microspheres from siloxane precursors with chemoresponsive indicators.

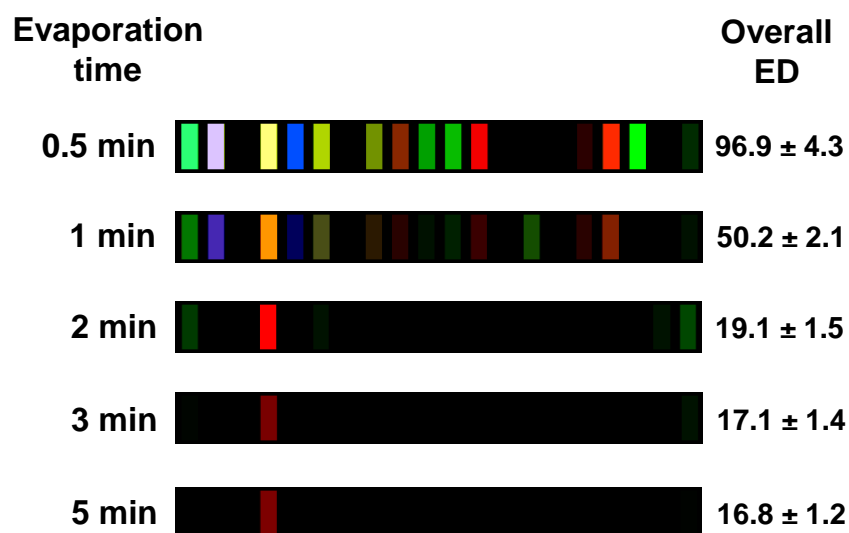


Figure S2. Validation of the evaporation process for the removal of volatile amines. Overall sensor response (defined as the Euclidean distance (ED) of the color changes in RGB values of the array sensors) goes down to a low and stable level after 2 min of evaporation at room temperature.

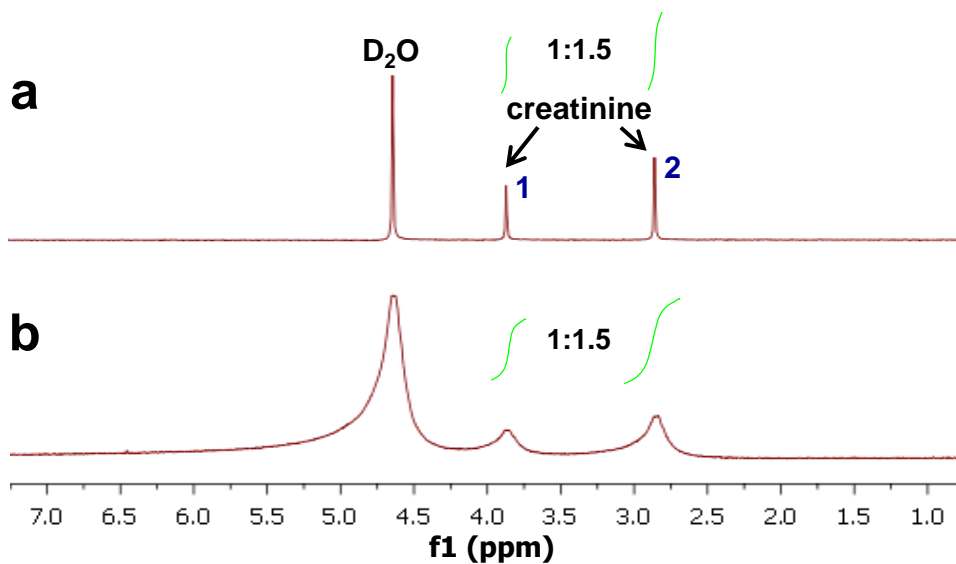


Figure S3. $^1\text{H-NMR}$ spectrum of creatinine solution (1 mg creatinine in 1 mL D_2O , ~ 10 mM) (a) without or (b) with the addition of Raney Ni (0.25 mg) and NaBH_4 (1 mg) and react for 10 min. The ratio of two peak areas (corresponding the methylene H and methyl H of creatinine) is 1:1.5 in both cases, and no new peaks appear after the addition of reductant. Peak broadening is due to the presence of paramagnetic species Ni.

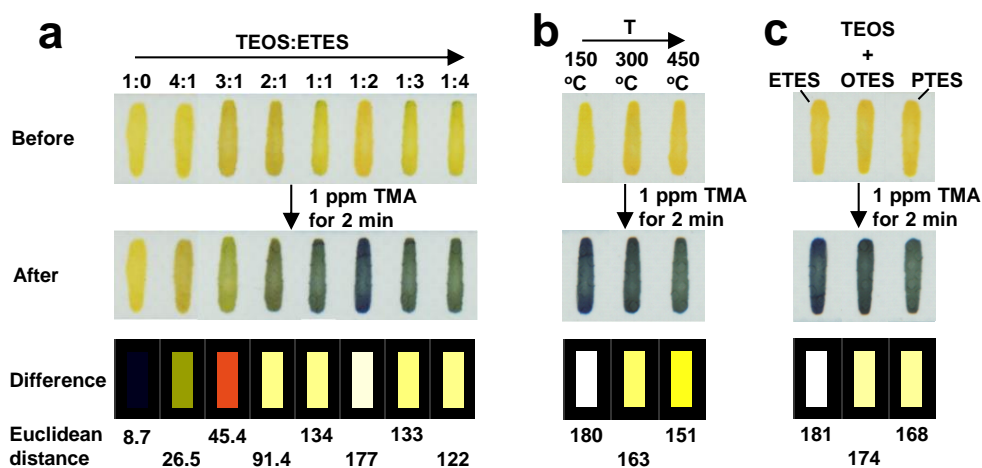


Figure S4. Before- and after-exposure images of printed silica-dye microspheres synthesized from (a) different molar ratios between TEOS and ETES at 150 °C, (b) 1:2 molar ratio of TEOS to ETES at different temperatures, and (c) 1:2 molar ratio of TEOS to one of three substituted triethoxysilanes at 150 °C. The sensor spots were exposed to 1 ppm TMA for 2 min in each case.

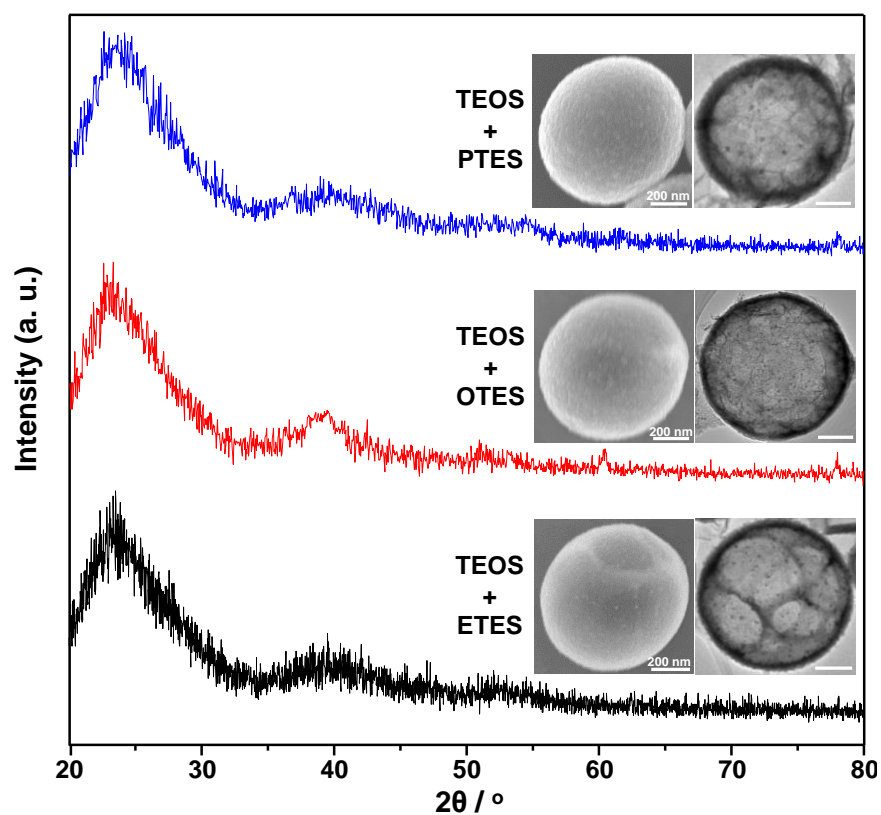


Figure S5. SEM, TEM images and XRD powder patterns of three silica-dye microspheres made from different siloxane precursors and bromocresol green. The broadness of the XRD powder patterns confirms the amorphous structures of all three microspheres. TEOS = tetraethoxysilane; ETES = ethyltriethoxysilane; OTES = octyltriethoxysilane; PTES = (2-phenylethyl)triethoxysilane.

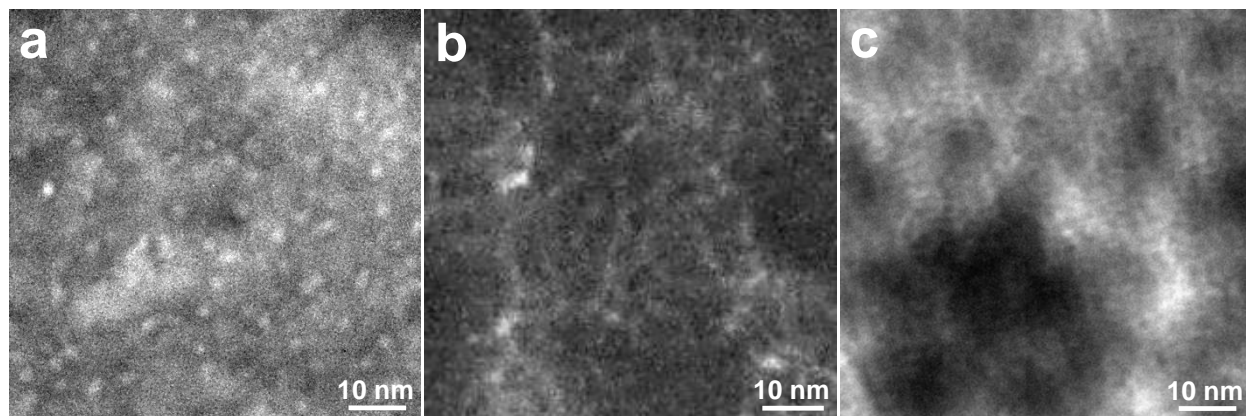


Figure S6. HR-TEM micrographs of three microspheres made from 1:2 molar ratio between (a) TEOS and ETES, (b) TEOS and OTES, and (c) TEOS and PTES. In (a), the light colored regions (1-2 nm in diameter) are low density regions corresponding to the high density of nanopores formed in the condensation of the sol-gel precursor during the USP process.

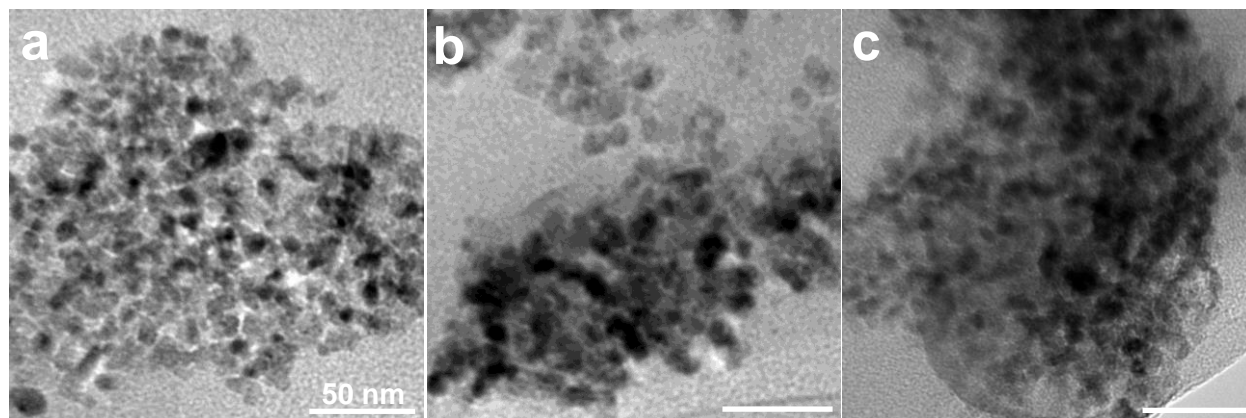


Figure S7. TEM micrographs of stirred silica-dye colloidal suspensions (i.e., not USP microspheres) made from the hydrolysis and condensation of 1:2 molar ratio mixtures between (a) TEOS and ETES, (b) TEOS and OTES, and (c) TEOS and PTES. No nanopores nor large BET surface areas were observed in these colloidal materials.

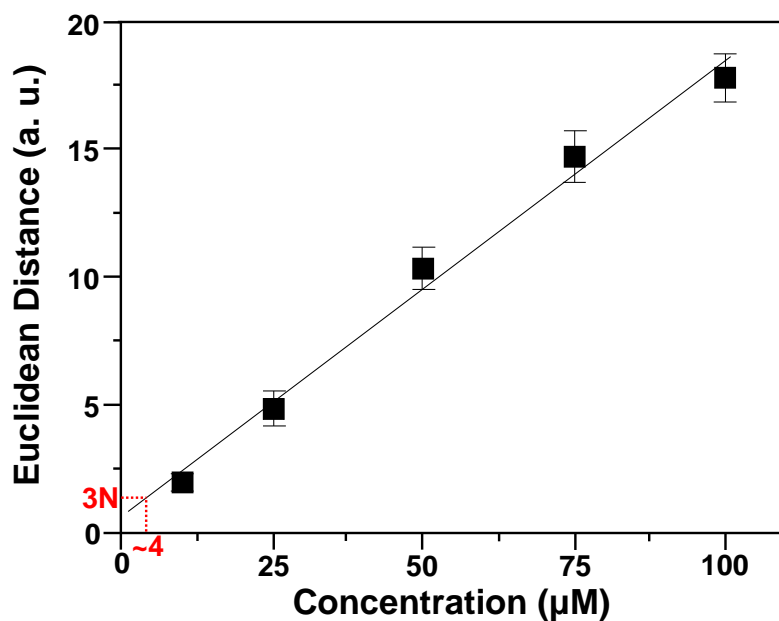


Figure S8. The calculation of the limit of detection (LOD) of urinary TMAO. Data points between 10 and 100 μM were linearly fit and extrapolated to the concentration when $S = 3N$ (S is defined as the sensor response, while N is defined as the standard deviation of all non-TMAO controls, which is ~ 0.47 Euclidean distance). The LOD is estimated to be $\sim 4 \mu\text{M}$.

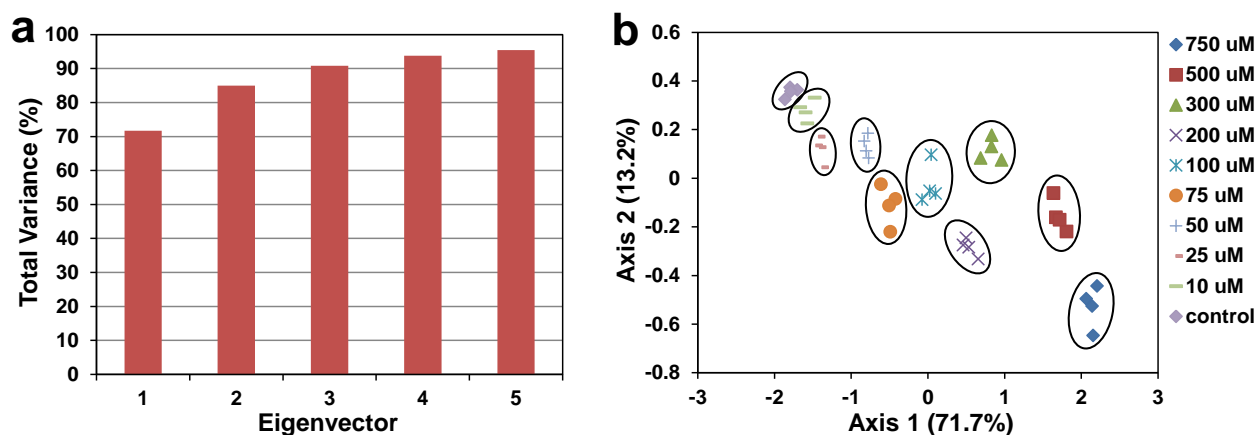


Figure S9. Principal component analysis (PCA) showing (a) scree plot of the distribution of total variance of each principal components, (b) score plot of all data points dispersed in the 2D space based on the top two principal components. Only a portion of the full dimensionality is captured in the 2D score plot (5 dimensions are required to include 95% of the total variance). Nonetheless, the PCA score plot shows clear grouping of different concentrations of TMAO (shown in key to Figure S9b on right) in the simulated urine samples.

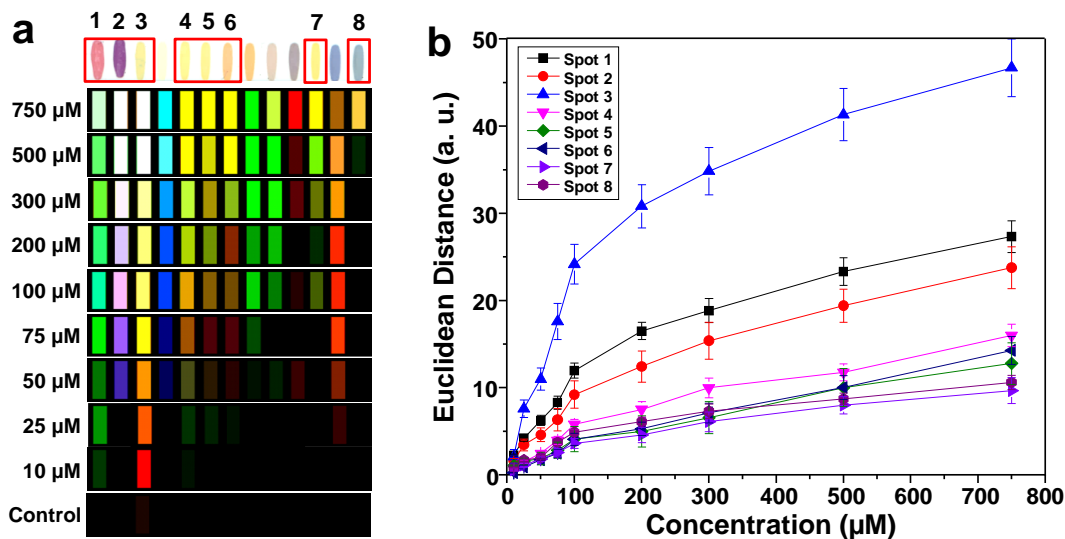


Figure S10. Sensor array optimization. The initial screening array (not shown here) had 20 different sensor formulations; 13 of the most promising were initially selected, and the responses of the best 8 sensor formulations are shown here. (a) The quantitative selection of 8 most responsive sensor spots (boxed in red) was accomplished by examination of their responses to TMA produced from the catalytic reduction of TMAO (as described in text) at the TMAO concentrations shown to the left; (b) Euclidean distance of each of 8 more responsive sensor spots as a function of TMAO concentrations. Spots 1 (containing α -naphthyl red) and 3 (containing tetraiodo-phenolsulfonephthalein) are the top two most responsive sensors.